Sea Ice Extents and global warming in Okhotsk Sea and surrounding Ocean

- sea ice concentration using airborne microwave radiometer -

Fumihiko Nishio
(Hokkaido Univ. of Education, Japan)

Abstract: Increase of greenhouse gas due to CO_2 and CH_4 gases would cause the global warming in the atmosphere. According to the global circulation model, it is pointed out in the Okhotsk Sea that the large increase of atmospheric temperature might be occurred in this region by global warming due to the doubling of greenhouse effect gases. Therefore, it is very important to monitor the sea ice extents in the Okhotsk Sea. To improve the sea ice extents and concentration with more highly accuracy, the field experiments have begun to compare with Airborne Microwave Radiometer (AMR) and video images installed on the aircraft (Beach-200). The sea ice concentration is generally proportional to the brightness temperature and accurate retrieval of sea ice concentration from the brightness temperature is important because of the sensitivity of multi-channel data with the amount of open water in the sea ice pack. During the field experiments of airborned AMR, the multi-frequency data suggest that the sea ice concentration is slightly dependending on the sea ice types since the brightness temperature is different between the thin and small piece of sea ice floes, and a large ice flow with different surface signatures. On the basis of classification of two sea ice types, it is clearly distinguished between the thin ice and the large ice floe in the scatter plot of 36.5 and 89.0GHz, but it does not become to make clear of the scatter plot of 18.7 and 36.5GHz. Two algorithms that have been used for deriving sea ice concentrations from airborned multi-channel data are compared. One is the NASA Team Algorithm and the other is the Bootstrap Algorithm. Intrercomparison on both algorithms with the airborned data and sea ice concentration derived from video images bas shown that the Bootstrap Algorithm is more consistent with the binary maps of video images.

1. Introduction

Many environmental issues on the earth might be caused by global warming due to the increase of greenhouse effect gases. It can be seen in the polar regions as the disintegrating and melting of glaciers and ice sheet by the atmospheric warming. In the Okhotsk Sea, where is located at the latitude between about 44° N and 60° N in the most southern region in the northern hemisphere and the sea ice is existing during winter season. According to global circulation model (GCM), it will be remarkably increasing the atmospheric temperature in the Okhotsk Sea region and therefore it is very important to investigate the sea ice extents and concentration of interannual variations in this region, and to predict how to provide sea ice changes occurred with the influence of global warming. Since the most comprehensive characterization of sea ice cover so far has been provided by satellite passive microwave data, we have begun the sea ice experiments with more accurate retrieval of sea ice concentrations, which has the same frequencies with the Advanced Microwave Scanning Radiometer (AMSR), launching on the platform Advanced Earth Observing Satellite-II (ADEOS-II).

This study is aiming to obtain the sea ice concentration derived from the airborne data being synchronized with AMR and the video image during same flight course. Among the most useful sea ice parameters that can be derived from passive microwave data, sea ice concentration, from which ice extent, the ice area, and the area of open water within the ice pack, can be calculated with the brightness temperature. The sea ice concentrations are derived by using a simple mixing algorithm of sea ice and for given ice temperature, the brightness temperature changes linearly with ice concentration. Two algorithms that have been used for retrieval of ice concentrations from multi-channel so far are, one is the NASA Team Algorithm and the other is the Bootstrap Algorithm, both of which were developed at NASA's Goddard Flight Center. To assess the difference in the performance of the two algorithm, the AMR data are applied to two algorithms to retrieve sea ice concentration in the Okhotsk Sea. The result of two algorithms intercomparison with the AMR data is shown to be suitable because the observed AMR data is indicating as brightness temperature difference by the difference signature of sea ice types. And hence, to extract sea ice concentration with signatures of sea ice types, the analyses are made to evaluate the combination of the better frequencies to be valid for the sea ice classification with using the combination of polarization. The NASA Team and Bootstrap Algorithm are also compared with available VTR images to be binary maps for corresponding sea ice concentration.

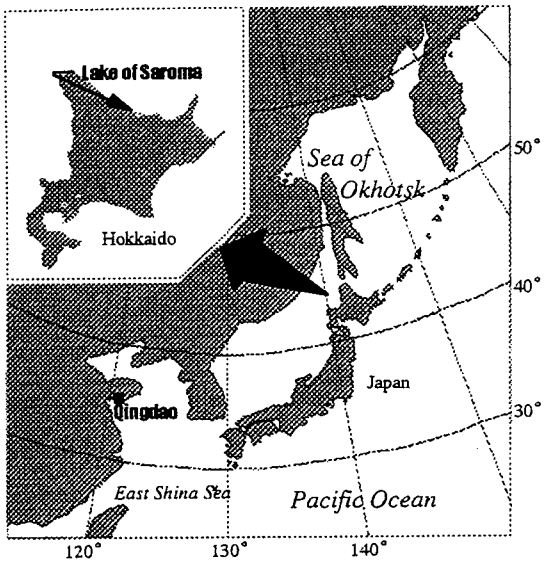

Fig.1 Locations of Sea of Okhotsk and Lake of Saroma.

2. Airborne Microwave Radiometer (AMR)

AMR is the microwave radiometer, which is the same channel with Advanced Microwave Scanning Radiometer (AMSR). The microwave radiometer installed airplane is receiving the energy scattered from the atmosphere and reflected from the surface of sea ice and sea water, and is expected to observe and receive a little energy mixtured from sea ice and open water surface in vertical and horizontal frequencies and polarized waves, and get line profiler with fixed horn antenna. The AMR data is calibrated by two point proofreading, high hot load and low temperature proofreading of liquid nitrogen cooling as cold load. The AMR data provide 12 channels of data 6.7, 10.65, 18.7, 23.8, 36.5 and 89.0 GHz for both H and V polarization, respectively. The characteristics of AMR sensors are shown in Table.1.

3. Field Experiments

Field experiments were carried out in the Lake of Saroma at the coast of Hokkaido Island in the Okhotsk Sea. The test site to obtain the sea ice parameters were chosen in the Lake of Saroma and the AMR data were archived along the flight line against winds and following the wind direction over the small part of Okhotsk Sea, where the surface is either covered or not covered by sea ice. All the sea ice is composed of the first-year ice, starting to freeze in the late autumn from early December to the end of May during winter season. In this field experiments, the AMR measures the brightness temperature of the sea water and sea ice, and retrieve sea ice extents and concentrations. Using these AMR data, this experiments are aiming to improve the sea ice concentration algorithm and develop the algorithm to exchange the AMSR data into some geophysical parameters.

4. Data Processing and Analysis

Table.1 Spec of AMR sensor

Antenna	Line profiler with fixed horn antenna					
Incident angle	55degree (fixed during flight)					
Frequency(GHz)	6.9	10.65	18.7	23.8	36.5	89.0
Band Width(MHz)	350	100	200	400	1000	1000
Beam Width El.	12.3	10	8.9	6.3	7.2	7.2
(3dB degree) Az.	10.7	8.6	6.5	5.4	6.2	6.2
Porarization	Vertical and Horizontal for all Frequency					
Receiver	Dicke switching reciever					
Integration Time	1.33sec					

START

1. Serect the suitable area for mosaicing
⇩
2. Make the movie-file
⇩
3. Divide the movie-file into some flames
⇩
4. Cut to be noize around the image
⇩
5. Retrieve the different of each image
⇩
6. Make the mosaic map
⇩
7. Make the AMR/EFOV image from mosaic map

END

Fig.2 Floe chart of making mosaic map

The AMR data are selected for the two flight courses of different sea ice types in Okhotsk Sea. One is the Course1-A exsisting thin and small piece of sea ice floes, the other is Course3-B, mostly a large ice floes. The image of these two flight courses is given in Fig.3., and these image made of one image which divide VTR image interval 1/10 seconds mosaic by mosaic soft.

4.1. Make the video image of sea ice

4.1.1. Mosaic image of video

This works makes mosaiced VTR image to retrieve sea ice concentration from AMR. VTR image which is filmed the sea ice condition under the airplane is inputted Power Mac 8500/180AV from video-board and is saved as 1sean 240x180 movie file of flame late 10 fps. The movie files are divided into some flames and are cut to be noise around the image. The processed image at 1 sean is 232x130. Developmental mosaiced soft in special calculate a difference data of position every 1 sean and then make the mosaiced image every 1 minutes referring to one. The floe chart of works are shown in Fig.2 and a sample image of mosaiced VTR image are shown in Fig.3.

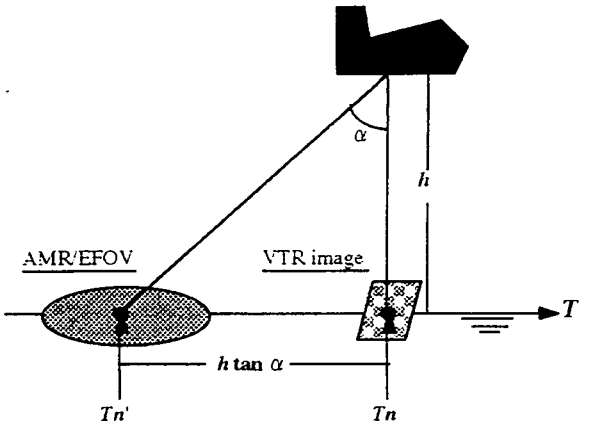

Fig.4 Relationship between the VTR image and AMR/EFOV center position.

4.1.2. Make the AMR/EFOV image on the mosaic image.

The method of determining AMR/EFOV (Effective Field Of View) center position to set the image of mosaiced VTR image use VTR time coordinates instead of not using GPS data. Because the output value of GPS data bring about the error to have a high speed in airplane. So, the accurate center position don't determine.

The mosaiced of VTR image use movie file of 10fps. The time of between some continuous movie-files are 1/10 seconds, and the relation is given by

$$T_1=T_0+1/10 \quad (1)$$

where T_0 and T_1 are VTR image time of a movie file and the next movie file. On the image after the mosaiced disposal, the coordinates of filmed time can be demanded by filmed time T_s of the first flame. Next, the center time coordinate T_n of the parameter n flames are given by

$$T_n=T_s+n/10 \quad (2)$$

So, the distance (D_n) from 1 flame to n flames are given by

$$D_n=v(T_n-T_s) \quad (3)$$

where v is the avarage flighe speed. The coordinate of the flight course use the filmed time T by VTR image and can be given by the equation (4) to express the time of VTR image.

$$D_n/v= T_n-T_s , \quad (4)$$

where, this equation can be expressed the flight distance from 1 flame to n flames by filmed time. So then, the distance from the center position of VTR image to AMR/EFOV Dn can express the flight altitude h and irradiance angle α of AMR horn antenna, and are shown in Fig.4 and given by

$$D_n=h\tan\alpha \quad . \quad (5)$$

Therefore, the center position of AMR/EFOV are expressed the filmed time of VTR image by dividing Dn ($=h \tan \alpha$) into v and given by

$$T_n'=T_n(h\tan\alpha)/v , \quad (6)$$

where Tn is time of AMR/EFOV center position. So AMR/EFOV center position correspond to the time coordinate on the mosaiced images. The AMR/EFOV

Course1-A *Course3-B*

Fig.3 A sample mosaic map of Sea of Okhotsk Sea. The mosaic maps are distribution of thin and small piece of sea ice floes in Course1-A and a piece of iceboard floes in Course3-B.

Table.2 This table is the Regression line's slope and Contributory Proportion(R^2) of each Courses. The best frequency to be grouping the sea ice types is the largest difference of two regression line's slopes and the biggest average of two R^2.

Frequency (GHz)		*Regression Line's slope*			*Contributory Proportion(R^2)*		
		Course1-A	*Course3-B*	*Difference:slope*	*Course1-A*	*Course3-B*	*Ave:R^2*
6.925	10.65	0.9002	0.8711	0.0291	0.9651	0.8739	0.9195
	18.7	0.901	0.9174	-0.0164	0.9367	0.9294	0.93305
	23.8	0.7519	0.7501	0.0018	0.907	0.8642	0.8856
	36.5	0.6786	0.6518	0.0268	0.9882	0.9373	0.96275
	89.0	0.3428	0.2049	0.1379	0.9833	0.882	0.93265
10.65	18.7	0.9726	0.9394	0.0332	0.9167	0.8461	0.8814
	23.8	0.81	0.768	0.042	0.8846	0.7866	0.8356
	36.5	0.7346	0.667	0.0676	0.9722	0.8523	0.91225
	89.0	0.3707	0.2017	0.169	0.9654	0.7827	0.87405
18.7	23.8	0.8147	0.7941	0.0206	0.9227	0.8771	0.8999
	36.5	0.7103	0.7035	0.0068	0.9382	0.989	0.9636
	89.0	0.3569	0.2133	0.1436	0.9237	0.8658	0.89475
23.8	36.5	0.8258	0.7809	0.0449	0.9122	0.8761	0.89415
	89.0	0.4174	0.2396	0.1778	0.9091	0.7854	0.84725
36.5	**89.0**	**0.5035**	**0.3026**	**0.2009**	**0.9885**	**0.8721**	**0.9303**

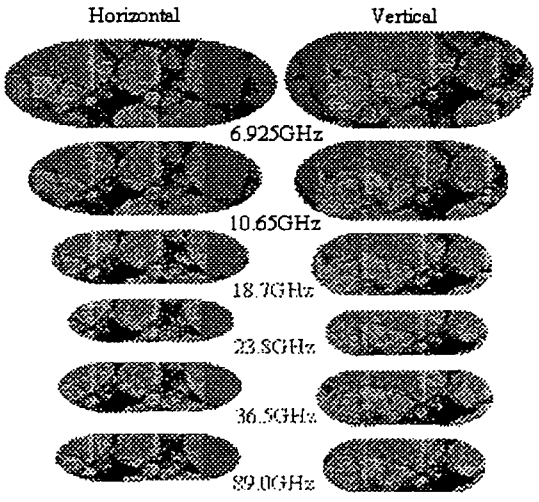

Fig.5 Sample mosaic map of AMR/EFOV area.

both ends coordinates for moving course are given by equation (7), and a sample image of AMR/EFOV area shown in Fig.5.

$$EFOV(s)_n = T_n - [1.33/2 + \{h\tan(\alpha + \theta/2)\}/v] \quad (7.a)$$

$$EFOV(e)_n = T_n + [1.33/2 - \{h\tan(\alpha + \theta/2)\}/v] \quad (7.b)$$

where the θ is the wide of beam, and the equation (7.a) and (7.b) are the times before and after the images of AMR/EFOV ares.

4.2. Sea ice concentration with two algorithms

The AMR data are applied to evaluate sea ice concentration with more accuracy, and it is to compare the sea ice concentration with VTR images. NASA team algorithm and Bootstrap algorithm were originally developed with using the Scanning Multichannel Microwave Radiometer (SMMR) and were improved on Special Sensor Microwave Imager (SSM/I). In this study, sea ice concentration is referred from VTR images and calculated by the total sea ice area as a binary map on the VTR mosaiced image, in which the footprint of VTR (EFOV: effective field-of-view) is projected.

4.3. Best frequency to sea ice

To make a selection of the better frequency and choose the polarized frequencies, regression line's slope and contributory proportion(R^2) by root mean square (RMS) are calculated by using the two flight course of AMR data. The best frequency to be grouping the sea ice types is the largest difference of two regression line's slopes and the biggest average of two R^2 as tabulated in Table2. The best frequency results from the combination of 36.5 and 89.0GHz for the airborned AMR data.

4.4. Sea ice concentration algorithm

1) The Bootstrap algorithm

Bootstrap algorithm technique (Comiso, 1995) is based on distributions of multichannel clusters of brightness temperature of sea ice. The sea ice concentration is derived from the scatter plot in the diagram of two frequencies of SSM/I, the vertically polarized 18.7 and 36.5GHz. The combination of 18.7V and 36.5V channels is shown in Fig.6. The sea ice concentration, C_i, corresponding to an observed brightness temperature, T_B, is derived from the mixing formulation and is given by

$$C_i = (T_B - T_W)/(T_I - T_W), \quad (8)$$

where T_W, and T_I are the brightness temperatures of open water and sea ice, respectively. Sea ice in this case may be on a mixture of the various ice types. Equation (8) could be applied to the appropriate values of T_W and T_I, which are determined from a combination of two channels as follows. The observed brightness temperature, T_B is expressed as the sum of contributions from two dominant ocean surface types difined by

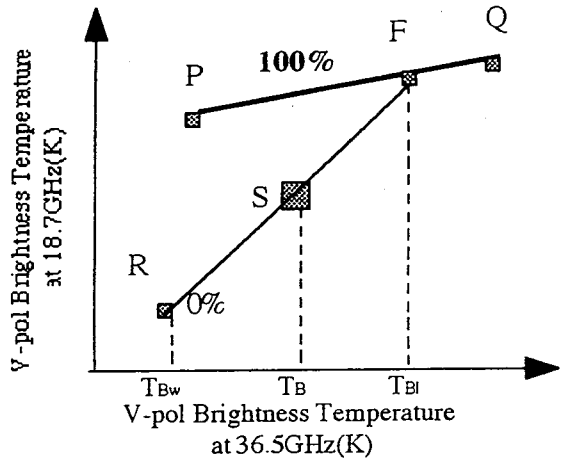

Fig.6 Bootstrap Algorithm

$$T_B=T_{BW}C_W+T_{BI}C_I, \quad (9)$$

$$C_W+C_I=1, \quad (10)$$

where T_{BW} and T_{BI} are the brightness temperature of open water and sea ice, respectively, and C_W and C_I, which is added to unity, are the corresponding fractions of each of the two ocean surface components within the field-of-view of the instrument.

2) The NASA team algorithm

The NASA team multichannel algorithm was originally developed to be used with Nimbus-7 SMMR radiances (Cavalieri et.al.,1984; Gloersen and Cavalieri,1986) but has subsequently been modified to be used with the DMSP SSM/I radiances as well (Cavalieri et.al.,1991). The microwave radiometer can distinguish the open water area within the sea ice pack with using the these characteristics of sea ice, which is that the difference of emissivity between the vertically and horizontally polarized radiances at 18.7GHz is small for either ice type in comparison with that for the ocean. The discrimination between first-year and multi-year ice is greater at 36.5GHz than 18.7GHz. The algorithm parameterizes these two characteristics through two radiance ratios that are used as independent variables (Cavalieri et.al.,1984). These are the polarization (PR) and the spectral gradient ratio (GR) difined by

$$PR=[T_{B(18.7V)}-T_{B(18.7H)}]/[T_{B(18.7V)}+T_{B(18.7H)}], \quad (11)$$

$$GR=[T_{B(36.5V)}-T_{B(18.7V)}]/[T_{B(36.5V)}+T_{B(18.7V)}], \quad (12)$$

where, for instance, $T_{B(18.7V)}$, $T_{B(36.5V)}$ and $T_{B(18.7H)}$ are the brightness temperatures at 18.7 and 36.5GHz vertical, and 18.7GHz horizontal polarization. The NASA Team algorithm is shown in Fig.7, which the value of PR distinguish open water from sea ice and GR distinguish from open water, first year and multi year ice. In Okhotsk Sea, it is the place which generate only first year ice, so the set of PR and GR is not including the multi year

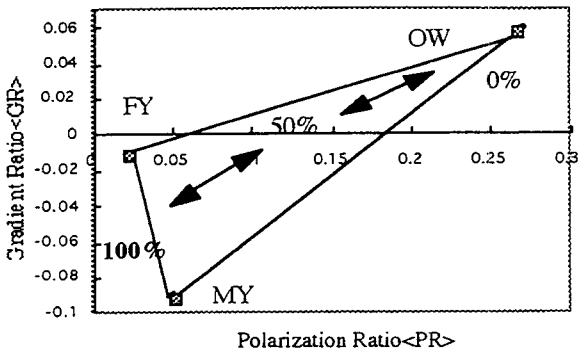

Fig.7 NASA Team Algorithm

ice. Then, sea ice concentration is abtained by dividing line, 0%-100%.

4.5. Intercomparison on the sea ice concentration using two algorithms

The brightness trmperatures at the frequencies of 18.7V and 36.5V, and 36.5V and 89.0V are analysed to obtain sea ice concentration from classification of the sea ice types in Bootstrap Algorithm, and also define NASA Team Algorithm using 36.5V/H and 89.0V, which make the algorithm of two vertical and horizontal frequencies. PR, GR is given by

$$PR=[T_{B(36.5V)}-T_{B(36.5H)}]/[T_{B(36.5V)}+T_{B(36.5H)}], \quad (13)$$

$$GR=[T_{B(89.0V)}-T_{B(36.5V)}]/[T_{B(89.0V)}+T_{B(36.5V)}], \quad (14)$$

where $T_{B(37V)}$, $T_{B(37H)}$ and $T_{B(89V)}$ are three brightness temperatures of 36.5V, 36.5H and 89.0V, respectively. The tie points of typical sea ice concentration at 0% and 100% are determined by brightness temperatures corresponded to the VTR images. At the brightness temperatures of 36.5V and 89.0V in Bootstrap algorithm, sea ice concentration is divided two types. In this analysis, the Course1-A data are calculated to retrieve the sea ice concentration and compared with the concentration derived from the VTR images. In the brightness temperatures of 18.7V and 36.5V, two regression lines are slightly distinguished between the two types of sea ice. However, in the Course3-B, the brightness temperatures at the large ice floes are higher than those at the thin and small piece of sea ice floes. On the other hand, NASA team algorithm is indicating as more scattered plot of first-year ice types in the diagram of PR and GR.

5. Conclusing remarks

Figure8(a) shows the Bootstrap algorithm using the brightness temperatures of 18.7V and 36.5V. The brightness tmperatures of thin and small piece of sea ice floes in the Course1-A is lower than that of a large ice floes in the Course3-B. The reason why the brightness

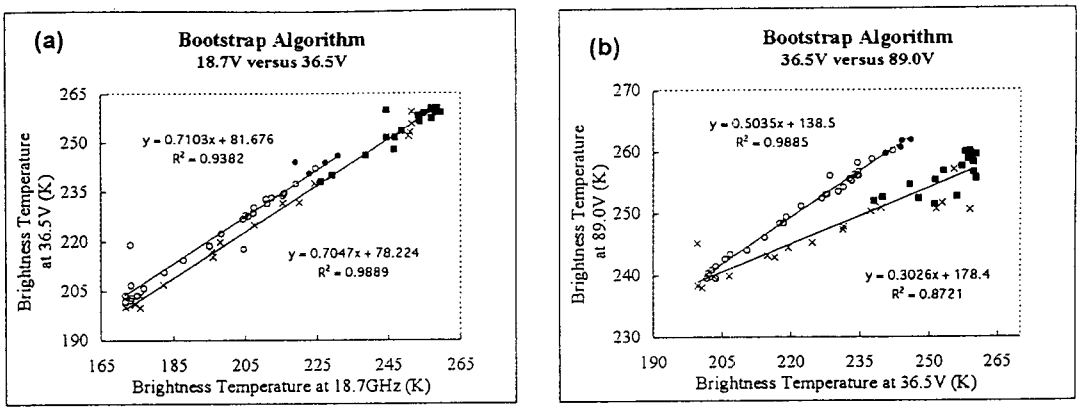

Fig.8 These graphs are Bootstrap Algorithm applied to brightness temperature of (a) 18.7- and 36.5GHz in vertical, (b) 36.5- and 89.0 GHz in vertical. These equations in each graphs are Regression line, and the line of plot ○● is Course1-A and plot ×■ is Course3-B. The plot●■ are sea ice concentration 100% in VTR image. On the graph(b), the set of 36.5- and 89.0GHz is grouping the sea ice types.

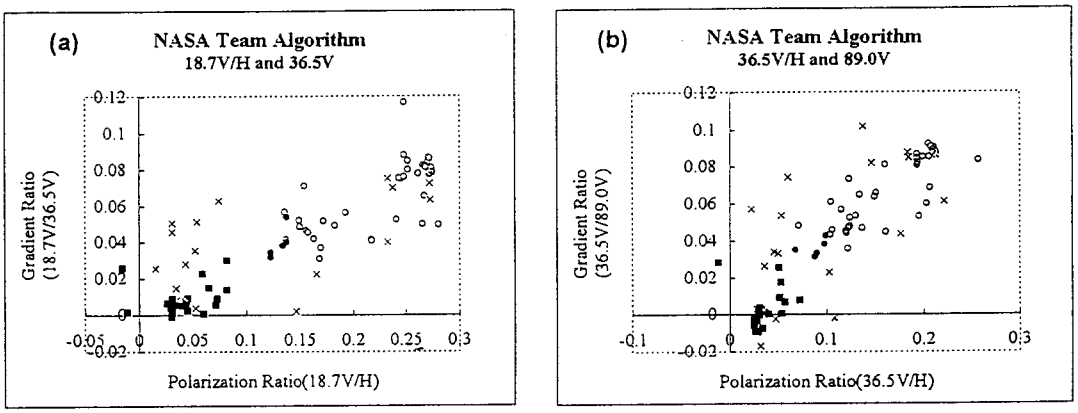

Fig.9 These graphs are NASA Team Algorithm applied to brightness temperature of (a) 18.7GHz in vertical and horizontal and 36.5GHz in vertical, (b) 36.5 GHz in vertical and horizontal and 89.0 GHz in vertical. The line of plot ○● is Course1-A and plot ×■ is Course3-B. The plot●■ are sea ice concentration 100% in VTR image. Each algorithm are also grouping sea ice types but sea ice concentration of Course1-A tends to be low.

temperature of sea ice in the Course1-A is lower than that of Course3-B is that the thin and small ice floes are soaked with the sea water by winds and waves, and is reduced to be smaller emissivity on the sea ice surface. So, the brightness temperature of Course1-A is lower to be covered with sea water of sea ice surface and to decrease sea ice emissivity. On the other hands, the sea ice in the Course3-B is a piece of iceboard floes, so it doesn't lean, upset and split, and the emissivity of this sea ice don't decrease. As the result of the Bootstrap algorithm of setting 18.7V and 36.5V, the brightness temperature is variable linearly according to sea ice types.

Figure8(b) shows the Bootstrap algorithm using brightness temperature of 36.5V and 89.0V. The brightness temperatures of thin and small piece of sea ice floes in the Course1-A, is lower only the brightness temperature at 36.5V than that of a piece of iceboard floes in the Course3-B. Because the brightness temperature is variable according to sea ice types, 89.0GHz is higher than the resolution at any other frequencies, so the brightness temperature at 89.0V don't decrease having no relation with sea ice types. As the result of the Bootstrap algorithm by 36.5V and 89.0V, the brightness temperature is distributed by the difference of sea ice types.

At the NASA team algorithm shown in Fig.9, each plot of (a),(b) is also scattered by the difference of sea ice types, and the plot of thin and small piece of sea ice floes in the Course1-A, is closely between the plot of a piece of iceboard floes and open water of sea ice concentration at 0%. In the Course1-A, the sea ice is existing the thin and small sea ice types, and the brightness temperatures at 18.7V,H and 36.5V is low because this sea ice types is influenced by sea water, winds and waves. So the those sea ice types are plotted toward open water of sea ice concentration at 0%. On retrieving sea ice concentrations, thin and small piece of sea ice floes have a tendency to be retrieved low concentrations.

In consideration on the above mentioned, Figure10 shows the correlation of sea ice concentration, which is the sea ice concentration of the footprint within VTR image (EFOV), the other is each algorithms. The best combination between VTR image and each algorithms is shown in Fig. 10(b). In the other combination in the Fig.10(a),(c) and (d), the sea ice concentration of each

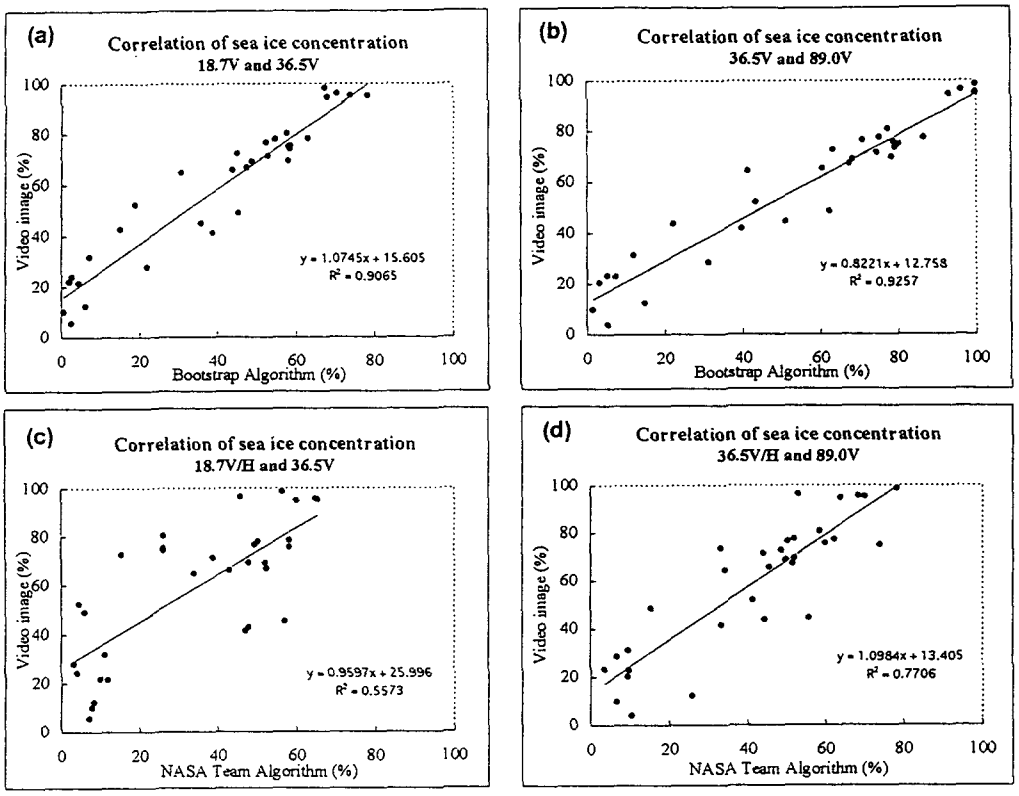

Fig.11 Correlation of sea ice concentration, VTR image versus each algorithm. The best combination of these algorithms is Fig11(b), VTR image versus Bootstrap algorithm of 36.5GHz and 89.0GHz in vertical, because sea ice concentration is demanded by sea ice type grouping.

algorithms is lower than that of retrieved by Bootstrap algorithm of 36.5V and 89.0V. In Fig.10(a), the Brightness temperature at Course1-A is lower than that at Course3-B, So sea ice concentration is indicated tend to be lower. On the other hand, the sea ice concentration of NASA team algorithm shown in Fig.10(c) and (d) is lower. The reason why that the sea ice concentration is lower is that the sea ice floes include the sea water and are distributed toward open water of sea ice concentration at 0% in spite of grouping the sea ice types. For instance, sea ice concentration at 100% of EFOV within VTR image, is distributed of the sea ice concentration out about 50% on NASA team algorithm.

In the Bootstrap algorithm of 18.7V and 36.5V shown in Fig.10(a), the sea ice types is grouping the same as each algorithm, but this algorithm retrieve the sea ice concentration with every different sea ice types. So the correlation of sea ice concentration show about y=x in the Fig.10(b). Sea ice concentration using AMR, the best algorithm retrieving sea ice concentration is the combination of brightness temperature at 36.5V and 89.0V.

On furtherworks, it is possible that the frequency at 89.0GHz installed on the ADEOS-II/AMSR. is influenced due to cloud and atmospheric vapor. So in the future, to analysis the influence of atmospheric vapor, the next step will be continued and carried out the sea ice observed by the AMR flight at an altitude of 10000ft, and will be compared the brightness temperature of the sea ice at 2000ft and 10000ft. The study is aiming to make the algorithm removing the influence of vapor. In the field experiments, the thin and small piece of ice floes includes the sea water, so this analysis examine the liquid water contents to measure the decrease of microwave radiation.

Reference

Josefino C.Comiso, Donald J.Cavalieri, Claire L.Parkinson, and Per Gloersen (1997): Passive microwave algorithms for sea ice concentration; A comparison of two techniques. *Remote Sens. Environ.* 60;357-384.

K.Cho, N.Sasaki, H.Shimoda, T.Sakata and F.Nishio (1996): Evaluation and improvement of SSM/I sea ice concentration algorithms for the Sea of Okhotsk. *J.Remote Sens. Soc.*

K.Oda, T.Kondo, M.Obata and T.Doihara (1998): Automated Mosaicing for Video Imagery Captured from Moving Platforms. *ISPRS Commission V Workshop 98*

M.Nakayama, F.Nishio, K.Cho, H.Enomoto and K.Imaoka (1997): Studies on ice concentration using airborne microwave radiometer in Okhotsk Sea. *Cold Region Technology Conference '97.*

M.Nakayama, F.Nishio, K.Cho, H.Enomoto, K.Imaoka, K.Oda and Y.Numata (1998): Evaluation effective field of view of airborne microwave radiometer using mosaiced image from VTR in Okhotsk sea ice. *Proceedings of the 24th Japanese Conference on Remote Sensing.*

Y.Huruhama, K.Okamoto and Y.Masuko (1986): Microwave remote senssing by satellite. *Japanese Society of Electronic communication*, p275. *Japan*, 16(2);p47-58.